



CENTRIFUGE MODEL TESTS ON SEISMIC RESISTANCE OF HIGH EMBANKMENT USING VOLCANIC COHESIVE SOIL

K. SAITOH, T. ISHII and N. KATAKAMI

NIKKEN SEKKEI Nakase Geotechnical Institute,
4-11-1 Minami-kase, Saiwai-ku, Kawasaki, Kanagawa 211, Japan

K. NOMOTO and T. SUGIMOTO

Ultra High Voltage Overhead Transmission and Substations Construction Office,
The Tokyo Electric Power Co., Inc.,
1274 Zaimoku-cho, Numata, Gunma 378, Japan

ABSTRACT

In order to ensure the stability of a high embankment during earthquakes, we propose the new method which is installed a core-block within the embankment. The numerical stability analysis for this embankment is performed by means of Fellenius method combined with the seismic coefficient method. Then, the calculated results were verified by the centrifuge model tests. The model embankment reduced to scale of 1/200 was applied a centrifuge acceleration of 200G. Immediately after the completion of consolidation due to its own weight, the model was applied horizontal force by the tilting table which simulated seismic coefficient method under this centrifuge acceleration, so as to investigate the behavior of failure in detail. The proposed method was found to improve its seismic resistance.

KEYWORD

Seismic Coefficient Method; Centrifuge Model Test; Slope Stability; Volcanic Cohesive Soil; Embankment.

INTRODUCTION

A site for a transformer substation has been developed in the slope accumulated volcanic cohesive soils and pyroclastic deposits. In the design for this project, an embankment with the maximum height of about 40 m had been decided to construct using volcanic cohesive soils in the site. In order to evaluate the embankment of stability analysis were performed by means of Fellenius method combined with the seismic coefficient method, taking account into the strength increase due to the self-weight consolidation. Figure 1 shows the critical circle and its safety factor for a design seismic coefficient of 0.15. This safety factor, 0.91, is lower than the allowable one of 1.20. Therefore, to stabilize the embankment, measures were designed to install the flat hexagonal core-block within the embankment using gravelly pyroclastic deposits in the same site, as shown in Fig. 2. Arrangements and shape of the core-block were designed to satisfy the allowable safety factors for three circular slip surfaces shown in the same figure and to minimize its volume. Furthermore, the dynamic analysis was performed to confirm the stability of the same embankment during earthquakes.

The embankment consists of remarkably different materials in compressibility, and is zoned into parts of complex shape. Moreover, the volcanic cohesive soils are classified into a special material in the geotechnical engineering,

and are a type of soil that is hard to assess the mechanical properties. Therefore, it is difficult to estimate the strength due to the self-weight consolidation and to evaluate the stability of the embankment by means of numerical methods. In this study, by using the static tilting table, which can physically reproduce the seismic method, attempts are made to establish the effectiveness of using this type of core-block in an embankment to improve its seismic resistance. In a series of centrifuge model tests, two types of model embankments with or without a core-block were used in order to confirm the effectiveness of a core-block during earthquakes. The model was reduced to scale of 1/200, prepared in the strong specimen box as shown in Fig. 3.

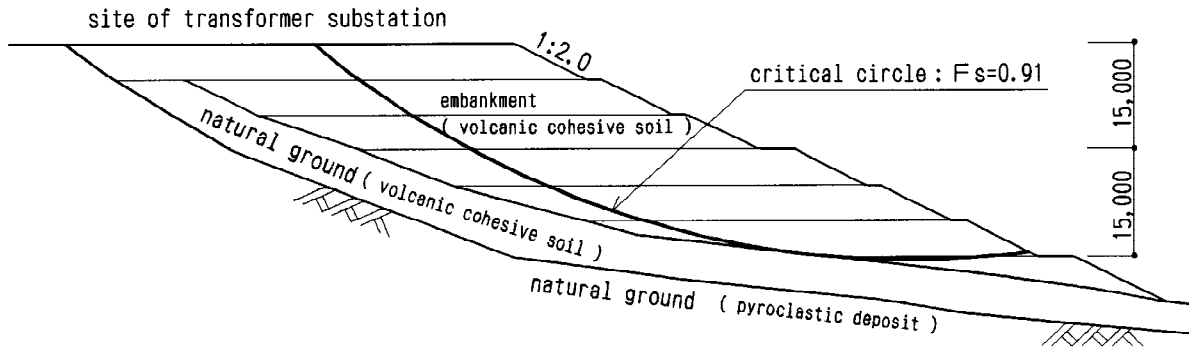


Fig. 1. Section of proposed embankment without a core-block and critical circular surface obtained by stability analysis during earthquakes (design seismic coefficient $k_h=0.15$, unit is mm)

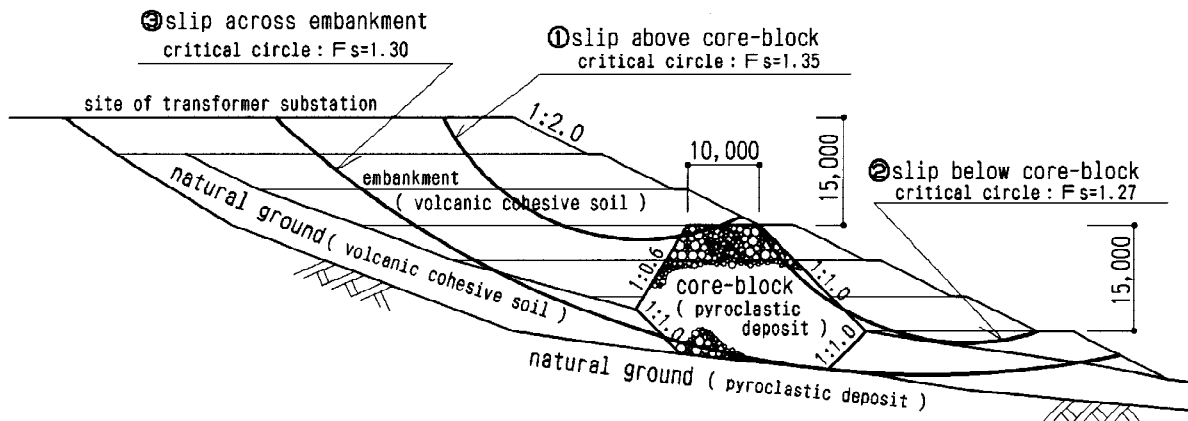


Fig. 2. Section of proposed embankment with a core-block and critical circular surface obtained by stability analysis during earthquakes (design seismic coefficient $k_h=0.15$, unit is mm)

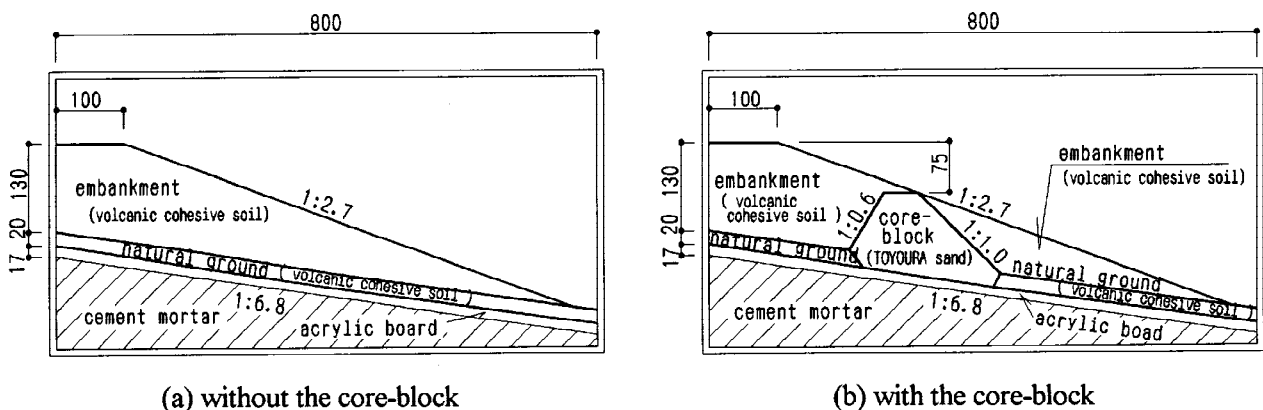


Fig. 3. Layout of model embankment with the core-block (model scale of 1/200, unit is mm)

MODEL PREPARATION

The model consisted of the embankment, the core-block, the natural grounds of the volcanic cohesive soil and the pyroclastic deposit as shown in Fig.3. Each part was prepared at the laboratory as follows.

Embankment; The material used for the model embankment was the volcanic cohesive soil sampled from the site. Its physical properties are as follows; Density of soil particles is 2.82 g/cm^3 , w_n 94.6 %, $F_c(<0.075\text{mm})$ 59 %, w_L 95 %, w_P 66 %, and I_p 29.

To determine the preparation method of the model embankment, the mechanical properties of rolling compacted volcanic cohesive soils were investigated by a series of triaxial compression tests $\bar{C}U$ and consolidation tests on the undisturbed and remolded samples. The undisturbed samples were taken from the test embankment constructed in the rolling compaction test at the site, the others were prepared in the laboratory. The rate of strength increase c_v/p obtained from $\bar{C}U$ -test on the undisturbed sample was 0.66, and that on the remolded samples was 0.59. Strength of the remolded sample is found to be slightly smaller than that of the undisturbed samples. Figure 4(a) shows the e - $\log p$ curves of the undisturbed samples. Each line is similar to others. The consolidation yield stress σ_y of all samples is approximately 90 kPa. These results suggest that the consolidation yield stress σ_y is the important index to reproduce the mechanical properties of rolled volcanic cohesive soil. Therefore, the model embankment was prepared by a statical compaction method as follows; The volcanic cohesive soil passed through a sieve of 9.5 mm was spread into the strongbox to a certain depth and was leveled. Then the pressure was applied on the loading platen inserted in the container. These processes were repeatedly conducted to a sufficient height. The spreading depth and the applied pressure were determined by a series of consolidation tests, to obtain the model embankment with the same consolidation yield stress as the embankment at the site. After several tests, it was found that the spreading depth and the pressure were 20 cm and 147 kPa, respectively. The e - $\log p$ curves of the model prepared in this condition is plotted in Fig. 4(a). Its consolidation yield stress and compression index are close to those of the test embankment.

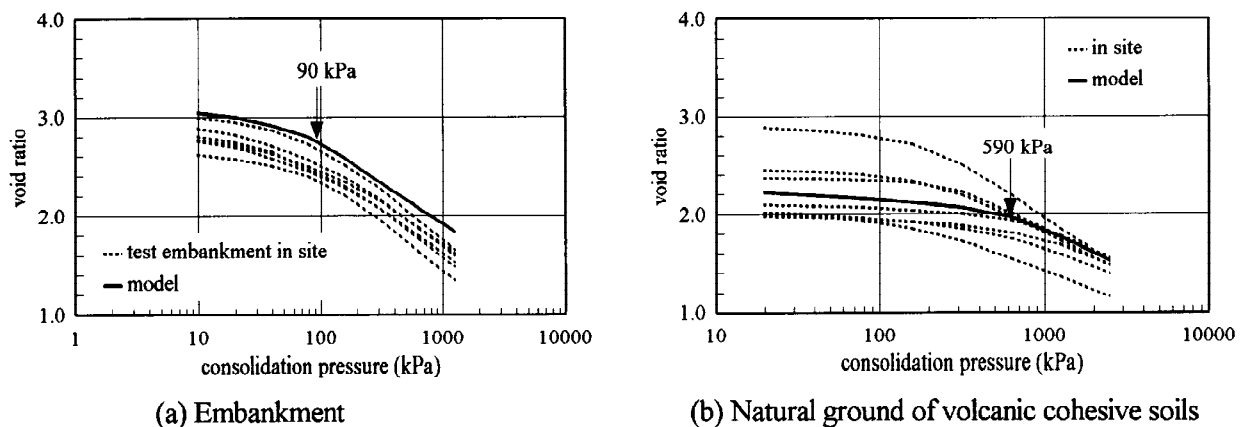


Fig. 4. e - $\log p$ curves of the undisturbed and remolded samples

Core-block; A material for the core-block in the design is demanded to have the internal friction angle ϕ_d of 39 degrees. The core-block material in the model tests was used Toyoura Sand which is a fine uniform sand having the average grain size, D_{50} of 0.16 mm and the density of soil particles, $\rho_s=2.65 \text{ g/cm}^3$. The reason why the material was selected was its well-known characteristics. Density of this sand was regulated so that strength of model was equivalent to that of the design values.

The model without the core-block was laid on its side, and an opening conformed to the shape of the core-block was made in the slope with paying attention to be disturbed. The opening was filled with the sand which was rained through the multiple sieve. Density of sand deposit in this process was determined in consideration of strength anisotropy (Tatsuoka, 1988), because the direction of accumulated deposit is not the same but normal to one of actual banking.

Natural ground of volcanic cohesive soil; The model natural ground illustrated in Fig.1 and Fig.2 was prepared by the same way of the model embankment as mention of before. The e -log p curves of the natural ground are shown in Fig. 4(b). The consolidation yield stress α_y was considered as 590 kPa from engineering judgment. From the same way as the embankment, it was decided that the spreading depth and the pressure were 10 cm and 628 kPa. The e -log p curve of the model prepared in this method is drawn in Fig. 4(b).

Natural ground of pyroclastic deposit; According to the previous soil explorations for the natural ground of the pyroclastic deposit shown in Fig.1 and Fig.2, its modulus of deformation E was approximately 110 MPa, remarkably large in comparison with the others. Its internal friction angle ϕ_d was about 40 degrees.

Furthermore, there was no critical circular slip surface passed this layer in the stability analyses. In considerations, the natural ground was modeled by the rigid acrylic board. The sandpaper was fixed on the surface of this board to be fasten on the upper layer.

STATIC TILTING TABLE

This table was gradually tilted in the plane of rotation of the centrifuge apparatus so as to simulate seismic method by the application of the horizontal force to the model. The seismic coefficient k_h is calculated from α -value using the equation of $k_h = \tan \alpha$, where the α is the angle of the tilting table from the horizontal plane. The capabilities of its equipment are as follows: The maximum value of the tilting angle is 20 degrees, the rate of tilting and the maximum payload of this table is 5 degrees/minute and 80 tons (Saitoh *et al.*,1995).

TEST PROCEDURE

After preparing the model, the side surfaces of the model were smeared with silicone grease film to reduce the friction against the walls of the strongbox. And then visual markers at the grid pattern with about 15 mm spacing were placed on the front surface of the model to observe the deformation of the model. Two displacement transducers were placed in the model to measure the vertical displacement at the crest of the embankment and the middle of the slope. The completion model was mounted on the static tilting table fixed onto a geotechnical centrifuge apparatus.

A procedure of this tilting table test is conducted as follows: First, a centrifuge acceleration is applied up to 200 G, so as to correspond to the construction process of the prototype embankment with the height of 40 m. After the model embankment was consolidated under a centrifuge acceleration of 200 G, the tilting table was gradually tilted in a rate of 4 degrees/minute until the embankment failed. Photographs of a model embankment were also successively taken through transparent side wall of the strongbox to obtain the deformation in detail.

TEST RESULTS

Deformation of the slope

The displacements of the model embankment were obtained from the coordinates of the markers on the photographs taken during the flight. The coordinates of them were read and digitized by means of a film projector, a screen digitizer and a data processor. Figure 5 shows the displacement loci of the model embankments without and with the core-block until failure. The embankment without the core-block distorted as seismic coefficient k_h increased, and the whole of failure across the slope suddenly happened at $k_h=0.16$. The observed failure surface was like a circular arc. The embankment with the core-block failed at $k_h = 0.34$ which was about twice as much as that without the core-block. This failure surface was a compounded pattern that passes along the core-block and through the middle of slope. It is found that the core-block prevents failure across the whole of slope and deformation of a slope above the core-block.

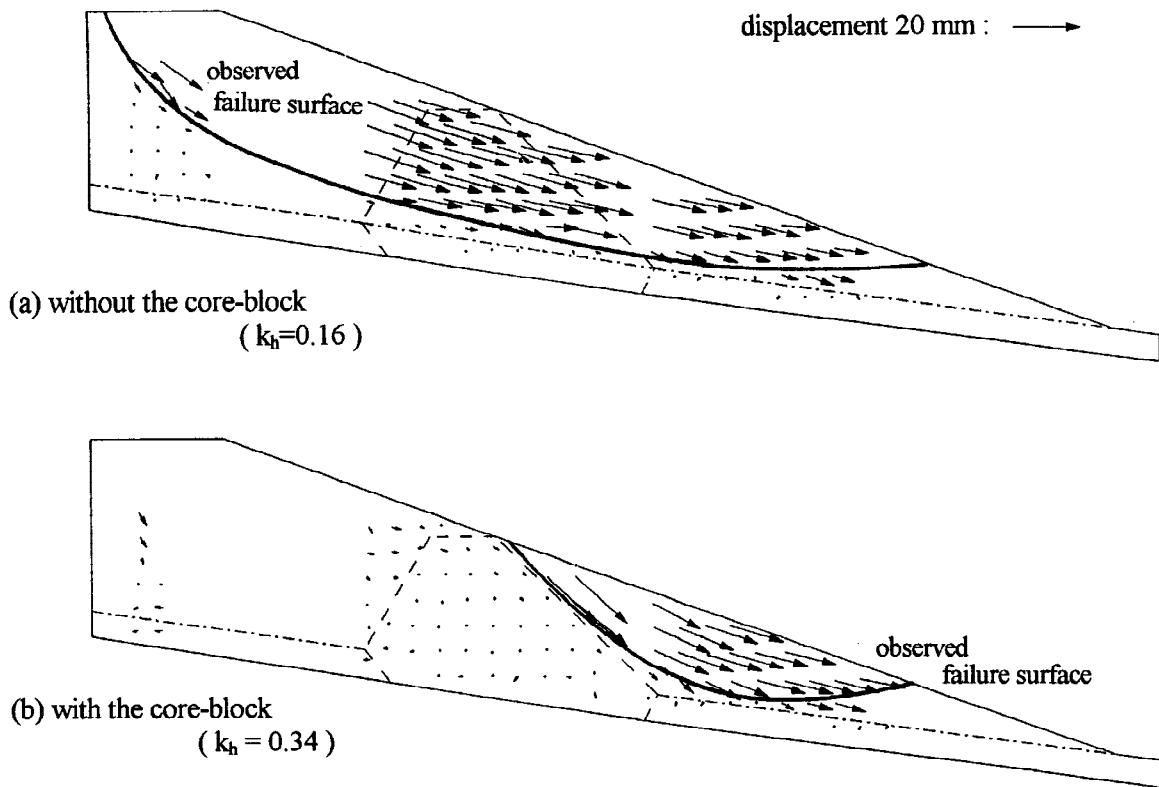


Fig. 5. Displacement loci of model embankment without and with the core-block during tilting until failure

Vertical displacement on the embankment

The relationships between seismic coefficient k_h and vertical displacements δ measured at the crest and middle of the embankment during tilting are shown in Fig.6. In the embankment without the core-block, two vertical displacements are not generated in the range of seismic coefficient less than 0.08. The vertical displacement increases gradually as seismic coefficient increases, and both the curves are inflected at seismic coefficient of nearly 0.12. When seismic coefficient exceeds that value, both changes in vertical displacements increase in the same, and the embankment suddenly fails. In the case of the embankment with the core-block, two vertical displacements are not generated in the range of seismic coefficient less than 0.11. Exceeding that value, increment

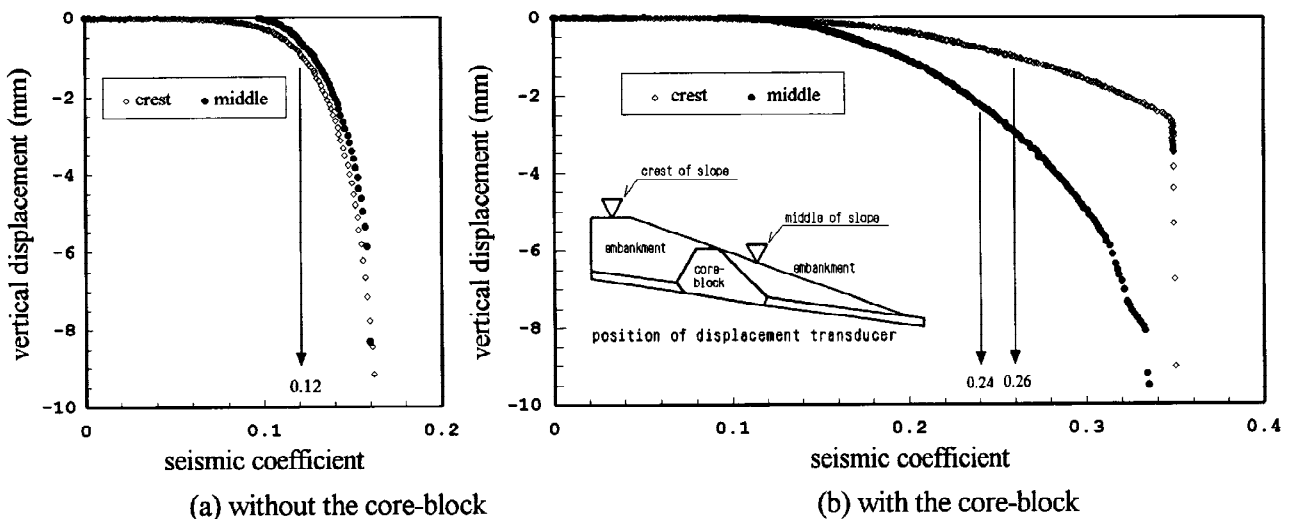


Fig. 6. Relationships between vertical displacements of embankment and seismic coefficient k_h

of displacement at the middle of the slope is larger than that at the crest. Finally the slope below the core-block failed at seismic coefficient of approximately 0.34. Immediately after this failure, the slope above the core-block has failed. The embankment with the core-block has a ductile characteristic in comparison with the embankment without the core-block, which characterized the larger strength and the following slow increase in deformation.

From the above discussion, it is found that the vertical displacement on the surface of the embankment is possible to estimate failure of the slope. Accordingly, the point of inflection on the relationship between seismic coefficient and vertical displacement on the surface of the embankment is expediently defined as seismic coefficient at the start of failure. In this way, the seismic coefficients at the start of failure are 0.24 and 0.12 for the embankment with the core-block and that without the core-block, respectively. Consequently the seismic resistance of the embankment with a core-block is about twice as large as that without the core-block.

Strain distribution in the embankment

Strains were calculated from relative displacements of markers to apply the procedure in FEM analysis, considering one triangular grid of markers as a triangular element with uniformed strain distribution. Figure 7 shows the distribution of the maximum shear strains γ_{max} of the embankment with the core-block at $k_h=0.33$ when was just before failure. The region of large shear strain corresponds to the location of observed failure surface which is drawn in this figure.

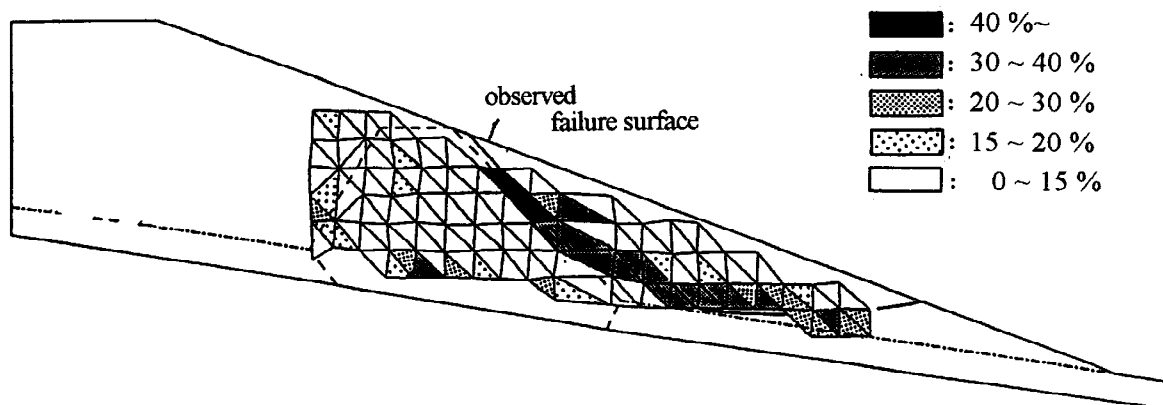


Fig. 7. Distribution of maximum shear strain with the core-block at $k_h=0.33$

Relationship between maximum shear strains and seismic coefficient

The relationship between shear strain and seismic coefficient for all of triangular elements were noticed to clarify when the failure starts and how the failure is progressive. Figure 8 shows the relationship for the element-73 and element-31 which are situated on observed failure surface. The maximum shear strains at both elements are almost constant to a certain seismic coefficient (0.11 for element-73, 0.18 for element-31), and rapidly increase as seismic coefficient increases over that. This rapid increment of shear strain happens in element-73 at smaller seismic coefficient than element-31. This indicates that element-73 fails before failure of element-31, and the growth of failure region is able to be obtained from this relationship. This seismic coefficient when the maximum shear strain rapidly increases is defined as that at the start of failure in the same way of the relationship between vertical displacement and seismic coefficient. According to this definition, the element-73 fails at $k_h=0.12$, and the element-31 fails at $k_h=0.21$.

Figure 9(a) and 9(b) show the distribution of seismic coefficient when the elements fail. These figures are drawn from the failure surface observed from the centrifuge model tests. It is reasonable that the failure surface passes the zone which has the relative small seismic coefficient. The elements on the failure surface in the embankment without the core-block have the seismic coefficient of about 0.13 at failure. These elements are found to fail at the same seismic coefficient. In the embankment with the core-block, the elements on the upper of the failure surface

fail at $k_h=0.13$. The seismic coefficient at failure increases gradually along the failure surface. As a result, the failure generates progressively.

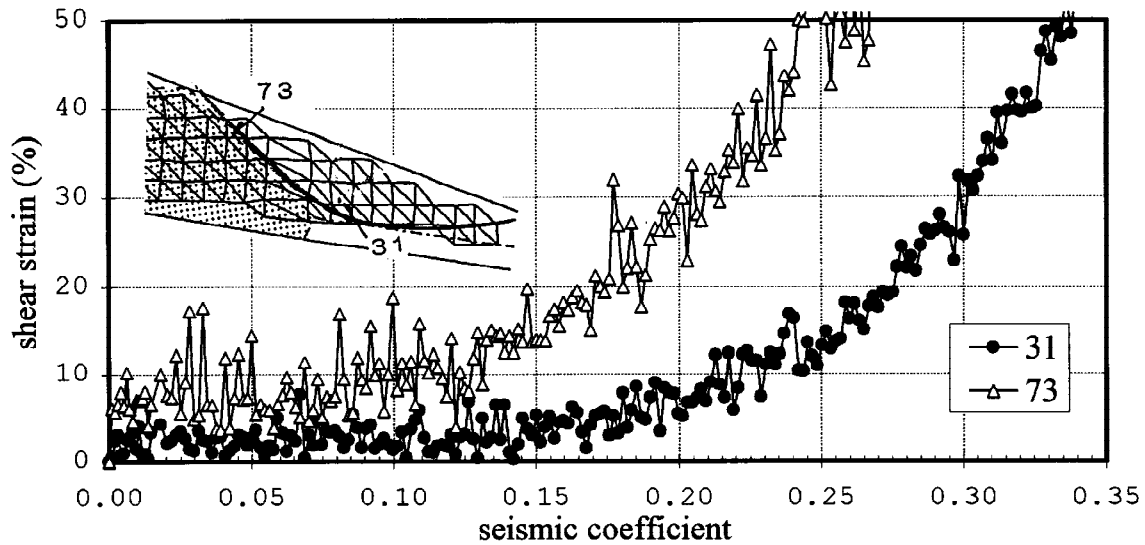


Fig. 8 Relation of maximum shear strain and seismic coefficient for embankment with the core-block

Seismic coefficient at start of failure

Table 1 shows the seismic coefficient at the start of failure obtained from the stability analysis and results of centrifuge model tests. The start of failure in calculation is defined as the safety factor to be equal to 1.0. Results of tests are obtained from the relationship between seismic coefficient ~ displacement curves and the seismic coefficient ~ maximum shear strain curves. The seismic coefficient when the slope was failed completely in tests is also shown together in this table. The table shows that there is little difference between results on the seismic coefficient at the start of failure. It is also found that the embankment with the core-block has about twice seismic coefficient as one without it. The seismic coefficient when the slope of the embankment without the core-block is failed completely is close to that at the start of failure. On the other hand, the embankment with the core-block has larger seismic coefficient at complete failure than that at the start of failure. The core-block improves the stability of the embankment.

Table 1 Seismic coefficient at start of failure

core-block	location of failure	calculation by Fellenius method	by centrifuge model test		
			from vertical displacement	from max. shear strain	at complete failure
without	entire slope	0.13	0.12	0.14	0.16
with	below core-block	0.26	0.24	0.23	0.34
	above core-block	-	0.26	-	0.35

Failure surface

The failure surface observed from the centrifuge model tests is compared with that obtained from the stability analysis. The failure surfaces for the embankment without and with the core-block are also drawn in Fig. 9(a) and Fig. 9(b), respectively. In the case of the embankment without the core-block (Fig. 9(a)), the observed failure surface corresponds well to calculated. Both failure surfaces pass across the whole of slope above natural ground of pyroclastic deposits, excepting that there is a slight difference in curvature near the crest and toe of the slope. In the embankment with the core-block, the observed and calculated failure happened in the slope below a core-block. But there is a difference in shape and location of the failure surface. The observed failure surface passes along the boundary between filling of volcanic cohesive soils and the core-block or the natural ground of volcanic cohesive soils. On the other hand, calculated failure surface passes through a core-block and the natural ground.

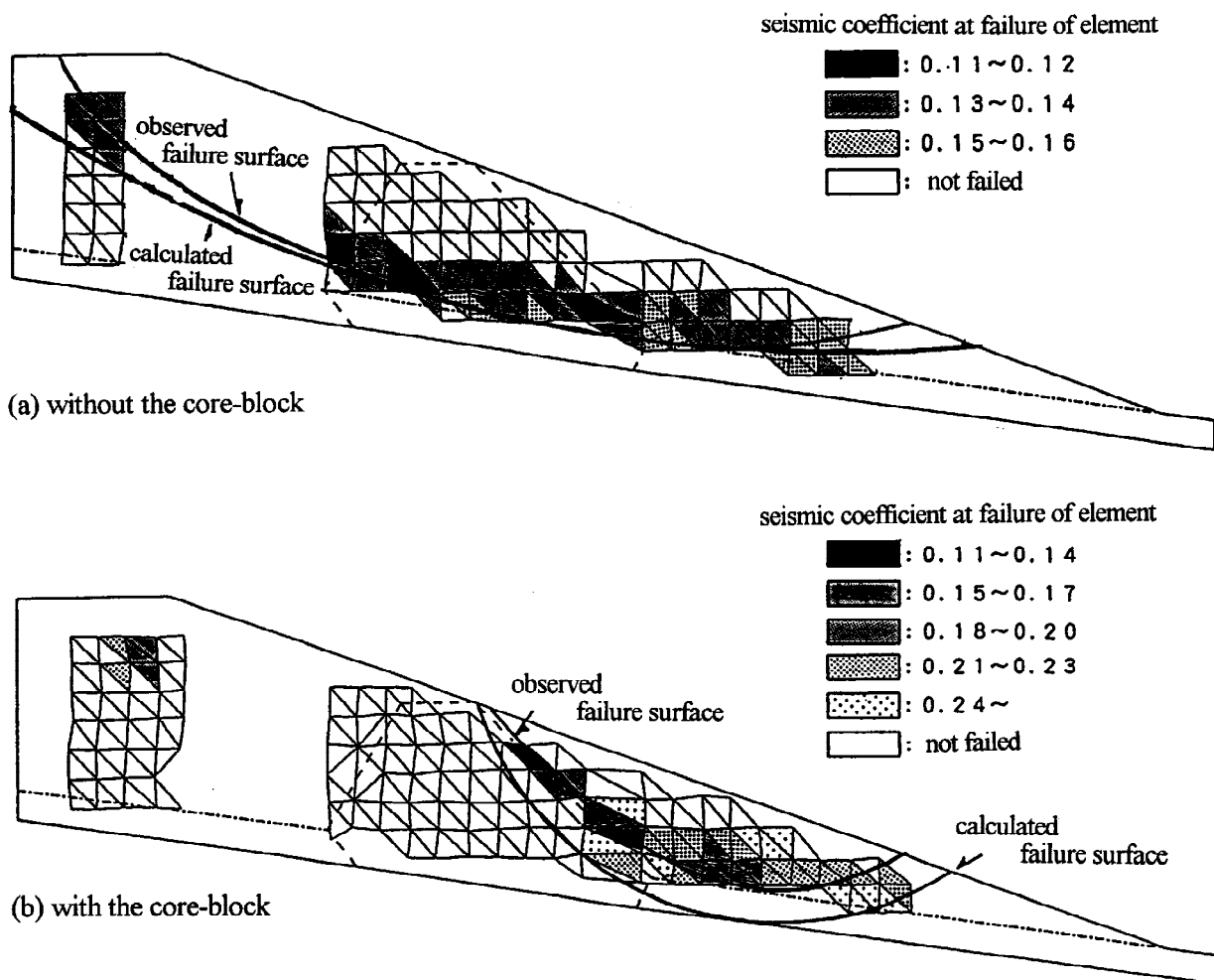


Fig. 9 Distribution of seismic coefficient when element fails and location of observed and calculated failure surface

CONCLUSION

A series of centrifuge model tests was performed to clarify the stability of the embankment proposed in the design and the effect of this type of slope protection. It is found that the core-block largely contributes to the stability of the embankment and the proposed design has a sufficient safety for the stability under specified seismic intensity. If the seismic resistance is evaluated by horizontal seismic coefficient at the start of failure, the embankment with the core-block is 0.26, which is about twice as that without it. The observed failure surface in the embankment with the core-block has a compounded pattern, which passes through the boundary between filling of volcanic cohesive soils and the core-block or the natural ground. These failures are found to take place progressively from the relations between maximum shear strain and seismic coefficient for all of elements. In addition, compared with the results of the stability analysis and the centrifuge model tests, both seismic coefficients at the start of failure are in good accordance.

REFERENCE

- Tatsuoka, F. (1988). Some recent developments in triaxial testing for cohesionless soils. *Advanced Triaxial Testing of Soil and Rock*, ASTM, STP 977.
- Saitoh, K., N. Katakami, T. Ishii, M. Tanaka, K. Nomoto and T. Sugimoto (1995). Development of a static tilting table for centrifuge. *Proc. 45th Annual Conf. of JSCE*, 3 (in Japanese).